energies

MDPI

Article

Assessment of the Use of Venetian Blinds as Solar Thermal Collectors in Double Skin Facades in Mediterranean Climates

Abel Velasco [1], Sergi Jiménez García [1], Alfredo Guardo [1,2,*], Alfred Fontanals [1] and Mònica Egusquiza [1,2]

[1] Centre de Diagnòstic Industrial i Fluidodinàmica, Universitat Politècnica de Catalunya BarcelonaTECH (UPC CDIF), Av. Diagonal 647, 08028 Barcelona, Spain; abel.velasco@estudiant.upc.edu (A.V.); sergi.jimenez.garcia@estudiant.upc.edu (S.J.G.); alfred.fontanals@upc.edu (A.F.); monica.egusquiza@upc.edu (M.E.)

[2] Càtedra JG per a l'Estudi de la Sostenibilitat d'Edificis, Universitat Politècnica de Catalunya BarcelonaTECH, Av. Diagonal 647, 08028 Barcelona, Spain

* Correspondence: alfredo.guardo-zabaleta@upc.edu; Tel.: +34-934015943

Received: 23 September 2017; Accepted: 7 November 2017; Published: 10 November 2017

Abstract: The global trend on energy integration and building efficiency is making both researchers and building developers look for technical solutions to use facade surfaces for energy harvesting. In this work, the assessment of the thermal performance of a double-skin facade (DSF) with a venetian blind-type of structure used as a solar thermal collector by means of computational fluid dynamics (CFD) is presented. A Venetian blind collector would allow for heat rejection/energy harvesting and exterior views simultaneously and can be easily integrated into the DSF aesthetical design. For the purposes of this study, the modeled facades (south, west, and east-oriented) were set to be located in Barcelona (Spain), where large solar gains are a constant condition throughout the year, and such large semi-transparent envelopes lead to interior over-heating in buildings, even during the winter. For the studied facades, both the reductions in radiative heat gains entering the building and the heat recovery in the Venetian blind collector were evaluated for a yearlong operation.

Keywords: double skin facades; computational fluid dynamics; solar thermal collector; energy integration; thermal performance analysis

1. Introduction

The efficient implementation and use of clean energy resources is one of the greatest challenges that we face as a global society. In recent years, we have witnessed a steady increase in global new investment in renewable energies (from 47 $BN during 2004 to 242 $BN during 2016). Only during 2016, wind, solar, biomass and waste-to-energy, geothermal, and small hydro and marine energy added 138.5 GW of installed capacity between them [1].

Another approach to clean energy use focuses on small scale energy harvesting (either using photovoltaic or solar thermal technologies) for local use in different building typologies. Buildings consume up to one-third of the total energy supply in developed countries, and up to one-fourth in developing countries [2]. In recent years, there has been a growing interest about the functionalization of building envelopes in order to reduce its energy consumption. This interest has strengthened the desire to use the building facade for the local production of electricity or the accumulation of thermal energy [3].

Building-integrated solar thermal (BIST) technologies can be a potential solution towards enhanced energy efficiency and reduced operational costs in contemporary buildings [4]. Solar thermal is the most mature technology among all currently available solar technologies, proving to have solar conversion

efficiencies two to four times higher than solar photovoltaic systems [2]. Furthermore, solar thermal technologies are of widespread use due to their wide range of applications and large-scale production at global level, assuring cheaper costs and shorter payback periods compared to its lifetime [5].

Double-skin facades (DSF) are a popular architectural trend, both for their attractive aesthetics and the improvement in internal comfort and building efficiency that can be achieved when used as a building envelope (by acting both as noise and thermal insulation) [6]. A DSF consists of two skins (a glazed outer layer and either a glazed or mixed inner layer) separated by an air cavity. The cavity can be ventilated (by either atmospheric openings or mechanical ventilation), and in some cases, shading devices might be installed into the cavity to reduce the solar heat gaining inside the building. In mild to cold climates (i.e., Northern Europe), it has been proven that the use of DSF reduces the heating loads during winter and increases the cooling loads of the building during summer [7]. However, in Mediterranean climates, where large solar gains and moderate to warm temperatures are a permanent condition throughout the year, DSF can lead to indoor overheating even during winter [8].

DSF are interesting due to their aesthetics or thermal insulation and their potential use as active solar facades (ASF). ASF, besides absorbing and reflecting the incident solar radiation, can also transform part of the absorbed radiation into electricity [9–11] or transmit the absorbed thermal energy into the building using mechanical equipment (e.g., pumps or fans on a hydraulic circuit). Quesada et al. [12] reviewed scientific studies carried out on transparent and translucent ASF during the first decade of this century. Recently, Zhang et al. [13] presented a comprehensive review on active solar thermal facades (ASTF).

Venetian blinds (VB) mounted behind glazed surfaces are typical shading devices used for daylighting control. VB also have a direct effect on indoor cooling loads and building energy consumption [14]. A VB-type of structure mounted in a closed-cavity DSF, besides serving its purpose as a shading device, can also be used as a heat exchanger, where the radiation heat absorbed on the VB louvers could be convected into a water stream circulating inside the slats forming the VB; this type of structure would allow for energy recovery and exterior views simultaneously, and can be easily integrated into the facade aesthetical design [15]. In this work the assessment, by means of computational fluid dynamics (CFD), of the thermal performance of a DSF with a venetian blind-type of structure, mounted in the DSF cavity and used as a solar thermal collector, is presented.

CFD has proven to be a useful tool on the study and optimization of DSF due to its ability to conjoint fluid dynamics, turbulence, thermal and radiation models into a single computer simulation, allowing to parameterize such complex multiphysics problem numerically [16]. Several authors have previously validated the use of CFD techniques when assessing the thermal performance of DSF. Manz [17] evaluated the total solar transmittance of a DSF with free convection using CFD techniques. Manz et al. [18] used CFD to evaluate the thermal performance of mechanically ventilated DSF. Windows and DSF with VB have also been studied by means of CFD modeling [19,20]. Previous work by this research group includes a CFD parametric study of the influence of construction and operation parameters on the thermal performance of a DSF [21], and a DSF with a VB [22].

CFD has also been used to model and validate the design of solar thermal collectors in order to obtain detailed information on the flow development and temperature distributions in the device. Previous works on this subject include the study of flat plate solar energy collectors [23,24], polymer solar collectors [25,26], solar collectors with horizontally inclined absorber strips [27], and tilted wavy solar collectors [28] on integrated collector storage devices [29,30], among others. In all the aforementioned cases, the authors found good agreement between theoretical and/or experimental analysis of the collectors and the obtained CFD simulation results.

For the purpose of this study, a one-storey DSF module with a VB mounted in its cavity (and acting as a thermal collector) was modeled using CFD. The modeled facades were set to be located in Barcelona, Spain, with orientation south, east, and west. For the studied facades, both the reductions in radiative heat gains entering the building and the heat recovery were evaluated for yearlong operating conditions. Thermal efficiencies were estimated for all studied cases.

2. Modeled Case

The geometric/numerical configuration used in this work is based on previous parametric studies in DSF with VB performed by this research group [8,15,21,22] in order to further analyze the thermal performance achieved by the proposed model. Previous studies were less comprehensive in their time scale (limited to estimate the facade performance during a single summer month), whereas the present work focus on the double skin facade-venetian blind (DSF-VB) model performance throughout a complete operation year.

2.1. DSF-VB Model

The control volume used for CFD simulations (Figure 1) consists of a one-storey ($4 \times 4 \times 0.28$ m) enclosed DSF module, and comprises (from outdoors to indoors) a 6 mm external glazed surface, a 280 mm enclosed cavity with VB and a 6 mm internal glazed surface. The closed cavity was taken to be filled with Nitrogen in order to avoid moisture condensation situations associated with enclosed air and glazing surfaces.

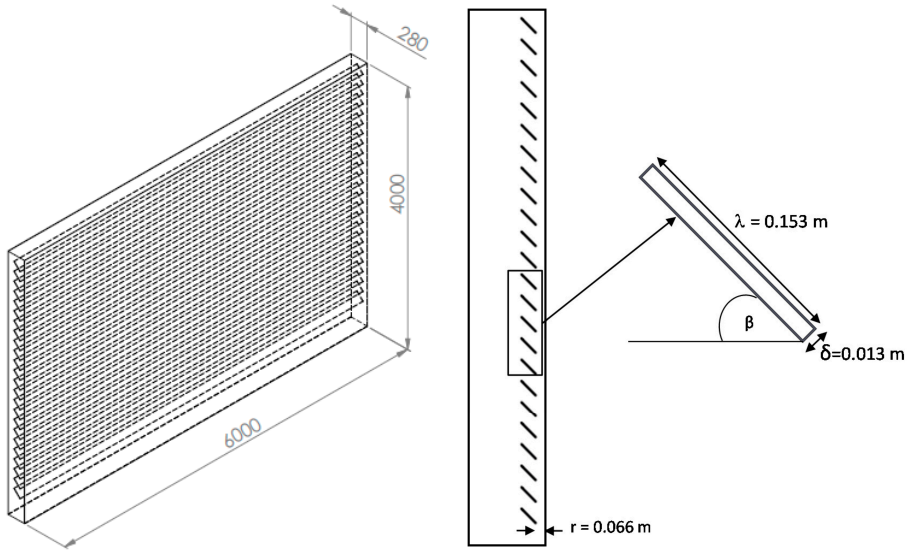

Figure 1. Geometry configuration for the double-skin facade (DSF) model.Left: Isometric view (dimensions in mm); Right: Vertical section.

A VB-type of structure consisting of 24 hollow aluminum slats, connected by 180° elbows forming a single hydraulic circuit, was placed in the DSF cavity. This structure acts as a solar thermal collector where the solar radiation absorbed by the slats is convected into a water stream circulating through the serpentine. VB louvers were taken to be hollow rectangular aluminum profiles with dimensions 153×13 mm and with a selective black surface treatment to assure high radiation absorptivity and low emissivity [31]. VB louvers tilt angle (β) was set to 45° to avoid glare issues due to direct day light reflection into the building at high solar elevation angles. For this study, the VB was placed at 6.6 cm from the external glazing [22].

An isometric view and general geometric configuration of the DSF-VB model used for this numerical study is shown in Figure 1. 180° elbows connecting the VB louvers are not shown in the figure.

2.2. Material Properties

Table 1 shows the physical and optical properties for all the materials used in the studied model. Thicknesses for the different layers were assigned following common practices in construction.

Table 1. Thermo-physical and optical properties of materials used in model elements.

Facade Element	ρ (kg/m^3)	μ (Pa·s)	c_p (J/kg·K)	k (W/m·K)	α	τ	ε
Exterior glazing	2500	-	795	1.16	0.15	0.78	0.89
Interior glazing	2500	-	795	1.16	0.15	0.25	0.05 (to bldg.) 0.89 (to cvty.)
VB louvers (Aluminum)	2719	-	878	169	0.80	-	0.15
Cavity (Nitrogen)	Ideal gas	Power law	1040	0.026	-	1	-
Water	998.2	0.001003	4182	0.6	-	-	-

2.3. Location and Climatic Conditions

The modeled building is assumed to be located in Barcelona, Spain (41.23 N–2.11 E). Climatic data (external air temperature) was obtained from Catalonia's meteorology agency [32], which provided raw hourly air temperature data from two different weather stations in Barcelona for the past 25 years. The external temperature data was hourly averaged and then fitted into a 6th-degree polynomial equation representing the hourly air temperature for an average day of each month of the year. Figure 2 shows an example of the polynomial fitting obtained for the external air temperature in Barcelona on an average day in July. Table 2 shows the polynomial regressions used to model the external air temperature for each month of the year. This time-dependent temperature profile was introduced as a boundary condition on the outer face of the exterior glass in our CFD software as a user-defined function.

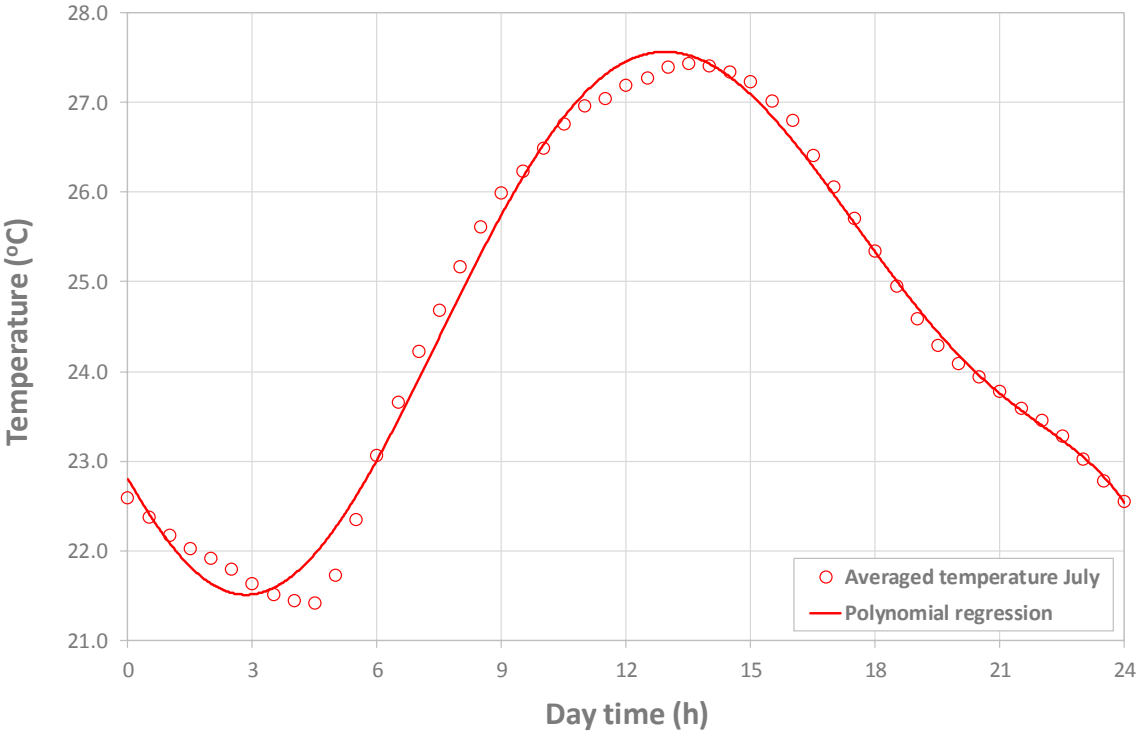

Figure 2. External air temperature for an average day of July in Barcelona.

2.4. Meshing

A tetrahedral grid was selected as the mesh to model the nitrogen inside of the cavity. Rectangular prisms were selected to model the glazed surfaces and the interior of the aluminum blinds. A refined mesh around all solid surfaces was set in order to properly model the thermal boundary layers created at the solid-fluid surface contacts. Mesh selection was based on geometrical parameters and previous work by this research group [21]. Figure 3 shows a detail of the cavity mesh near the external glazing and the louvers.

Table 2. Polynomial regressions for the average external air temperature (T, in °C) as a function of day time (t, in s) in Barcelona.

Month	Polynomial	R^2
January	$T = -3.878\times10^{-27}t^6 + 1.054\times10^{-21}t^5 - 1.060\times10^{-16}t^4 + 4.740\times10^{-12}t^3 - 8.807\times10^{-8}t^2 + 5.269\times10^{-4}t + 7.546$	0.9666
February	$T = -3.717\times10^{-27}t^6 + 1.007\times10^{-21}t^5 - 1.003\times10^{-16}t^4 + 4.384\times10^{-12}t^3 - 7.686\times10^{-8}t^2 + 4.002\times10^{-4}t + 7.456$	0.9881
March	$T = -3.694\times10^{-27}t^6 + 9.727\times10^{-22}t^5 - 9.340\times10^{-17}t^4 + 3.864\times10^{-12}t^3 - 6.123\times10^{-8}t^2 + 2.667\times10^{-4}t + 9.844$	0.9907
April	$T = -2.871\times10^{-27}t^6 + 7.359\times10^{-22}t^5 - 6.726\times10^{-17}t^4 + 2.505\times10^{-12}t^3 - 2.920\times10^{-8}t^2 + 1.463\times10^{-5}t + 12.61$	0.9920
May	$T = -2.064\times10^{-27}t^6 + 5.141\times10^{-22}t^5 - 4.393\times10^{-17}t^4 + 1.344\times10^{-12}t^3 - 2.757\times10^{-9}t^2 - 1.787\times10^{-4}t + 15.34$	0.9895
June	$T = -1.004\times10^{-27}t^6 + 2.453\times10^{-22}t^5 - 1.895\times10^{-17}t^4 + 3.125\times10^{-13}t^3 + 1.576\times10^{-8}t^2 - 3.079\times10^{-4}t + 19.82$	0.9875
July	$T = -1.224\times10^{-27}t^6 + 3.075\times10^{-22}t^5 - 2.611\times10^{-17}t^4 + 7.279\times10^{-13}t^3 + 4.398\times10^{-9}t^2 - 2.227\times10^{-4}t + 22.80$	0.9903
August	$T = -1.619\times10^{-27}t^6 + 4.150\times10^{-22}t^5 - 3.786\times10^{-17}t^4 + 1.369\times10^{-12}t^3 - 1.199\times10^{-8}t^2 - 1.037\times10^{-4}t + 23.62$	0.9885
September	$T = -1.789\times10^{-27}t^6 + 4.590\times10^{-22}t^5 - 4.248\times10^{-17}t^4 + 1.620\times10^{-12}t^3 - 1.861\times10^{-8}t^2 - 5.894\times10^{-5}t + 20.86$	0.9895
October	$T = -2.305\times10^{-27}t^6 + 5.878\times10^{-22}t^5 - 5.447\times10^{-17}t^4 + 2.134\times10^{-12}t^3 - 2.876\times10^{-8}t^2 + 1.694\times10^{-5}t + 17.56$	0.9866
November	$T = -2.312\times10^{-27}t^6 + 6.121\times10^{-22}t^5 - 5.941\times10^{-17}t^4 + 2.503\times10^{-12}t^3 - 4.086\times10^{-8}t^2 + 1.798\times10^{-4}t + 12.18$	0.9870
December	$T = -2.735\times10^{-27}t^6 + 7.388\times10^{-22}t^5 - 7.360\times10^{-17}t^4 + 3.228\times10^{-12}t^3 - 5.711\times10^{-8}t^2 + 3.039\times10^{-4}t + 8.861$	0.9860

Mesh independency tests were run for both the cavity and the louvers mesh, imposing constant radiation heat fluxes as boundary conditions and monitoring temperature profiles. Mesh-independent results were obtained for mesh sizes of 4173 kEl for the cavity and 2630 kEl for the louvers [33].

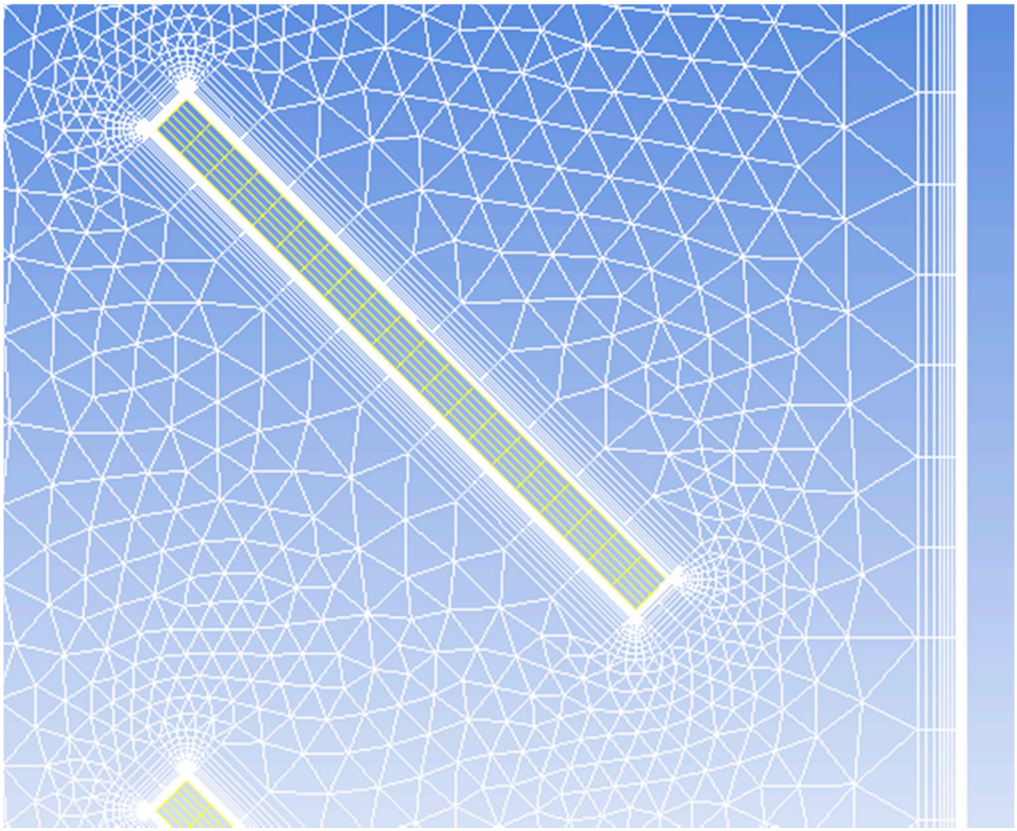

Figure 3. Detail of the cavity mesh.

2.5. Parametric Study

In order to evaluate the influence of certain construction and operating parameters, a parametric study was carried out by means of a set of CFD simulations varying the cavity width, the interior glazing reflectivity, and the water velocity through the VB louvers. The improvement on the DSF-VB thermal collector performance was assessed by measuring the reduction on the solar heat gains through the interior glazing of the DSF-VB module when compared to a base case.

For all the cases studied, the heat flux through the interior glazing was recorded for 1-day operation. Climatic and radiation conditions were set to those of 15 July, around where peak solar radiation is expected for the location.

Table 3 shows the studied cases and the obtained results. The first row of each parameter studied corresponds to the values selected for the base case. As expected, lower solar heat gains were obtained when a higher flow rate circulates through the VB louvers. In addition, heat gains were reduced by increasing the reflectivity of the interior glazing. Decreasing the cavity width, on the contrary, increases the heat gains as it reduces the global heat transfer coefficient of the module. For the purposes of this study, Re = 16,000, an interior glazing reflectivity of 60% and a cavity depth of 280 mm was selected for all forthcoming simulations.

Table 3. Solar heat gains (kJ/m^2/day) obtained for the parametric study.

Water Flow Rate (Re)		Interior Glazing Reflectivity (γ)		Cavity Depth (w)	
Parameter	**kJ/m^2/day**	**Parameter**	**kJ/m^2/day**	**Parameter**	**kJ/m^2/day**
Re = 4000	936.17	γ = 0.80	936.17	w = 280 mm	936.17
Re = 8000	854.12	γ = 0.60	1072.83	w = 212 mm	1078.96
Re = 12,000	851.92	γ = 0.35	1480.19	w = 146 mm	1450.48
Re = 16,000	764.91	γ = 0.10	1625.91		

2.6. Boundary Conditions and Solver Set-Up

The studied cases were taken to be a conduction/convection/radiation heat transfer problem involving two fluid zones: an enclosed cavity (filled with nitrogen) and a serpentine (water running through the hollow louvers).

In order to simulate the studied cases, Navier-Stokes equations together with the energy conservation equation were solved using CFD code Ansys Fluent® v16. RNG k-epsilon turbulence model (for the serpentine), a laminar flow model (for the enclosed cavity), and P1 radiation model were selected as numerical sub-models for all cases tested.

A pressure-based double-precision transient solver was selected in order to solve the set of equations used. Second order upwind discretization schemes were imposed on all the transport equations. PISO pressure-velocity coupling was chosen due to its suitability for buoyancy-affected flows. The fluid was taken to be incompressible, Newtonian, and in laminar or turbulent flow regime, depending on the fluid zone. All the numerical sub-models, discretization and simulation strategies were previously validated against an experimental database [21]. A time step of 120 s was selected for the transient simulations.

Boundary conditions were set as close as possible to DSF regular operating conditions. Time-dependent external air temperature was imposed using a user-defined function based on the polynomial regression discussed in Section 2.3. Solar radiation dynamics (including the estimation of direct, diffuse and ground-reflected radiation) were simulated using Ansys Fluent v16 Solar Calculator, which estimates the position of the sun with respect to the numerical model for every simulation time step. The superficial velocity of the water running through the aluminum louvers, the cavity depth and the interior glazing reflectivity and emissivity toward the building interior were set according to the parametric study shown in Section 2.5.

Thermal boundary conditions for the exterior and interior glazing were imposed as convective and radiative heat fluxes and convective heat flux respectively. Convection coefficients were set to 12 W/m^{2}K and 8 W/m^{2}K for the outdoors and indoors glazing surfaces, respectively, and the building interior temperature was set to 22 °C during the winter/25 °C during the summer following Spain's regulations on energy efficiency in buildings [34].

Nitrogen density and viscosity were set as temperature-dependent. Material physical and optical properties were set as shown in Table 1. Water inlet temperature and cavity initial temperature (at simulation start time) was set to 25 °C (from April to October) or 22 °C (from November to March) to match the selected building interior temperature.

For the South-oriented facade, the simulation time range was set from before sunrise to about sunset for each studied case, for the East-oriented facade the time range comprised from before sunrise

until the solar midday, and for the West-oriented facade, this time range went from the solar midday to about sunset for each studied case. Table 4 shows the initial/final simulation times for all studied cases.

Table 4. Initial/final simulation times.

Month	Sunrise	Sunset	South Facade		East Facade		West Facade	
			Start Time	End Time	Start Time	End Time	Start Time	End Time
January	8:06	18:03	7:00	18:00	7:00	13:00	12:00	18:00
February	7:31	18:38	7:00	18:00	7:00	13:00	12:00	18:00
March	6:40	19:13	6:00	19:00	6:00	13:00	12:00	19:00
April (DST)	6:53	20:45	6:00	20:30	6:00	13:30	13:00	20:30
May (DST)	6:22	21:16	6:00	22:00	6:00	14:00	13:00	22:00
June (DST)	6:17	21:29	6:00	22:00	6:00	14:00	13:00	22:00
July (DST)	6:20	21:29	6:00	21:00	6:00	14:00	13:00	21:00
August (DST)	6:44	21:11	6:00	21:00	6:00	14:00	13:00	21:00
September (DST)	7:15	20:28	7:00	20:00	7:00	14:00	13:00	20:00
October (DST)	7:45	19:37	7:00	19:30	7:00	13:30	13:00	19:30
November	7:20	17:49	7:00	18:00	7:00	13:00	12:00	18:00
December	7:55	17:30	7:00	18:00	7:00	12:30	12:00	18:00

Numerical simulations were performed using up to 24 cores on a Hybrid Bull machine (Barcelona, Spain) (240 cores/20 processors Intel Xeon E5-2697 @ 2.7 GHz (12 cores/processor)/10 Intel Xeon Phi 5120P coprocessors/2.8 TB), property of Consorci de Serveis Universitaris de Catalunya (CSUC). Simulation times ranged from 65 to 120 core hours depending on the studied case. Numerical convergence of the model was checked based on the normalized numerical residuals of all computed variables, set to 1×10^{-5} for mass, momentum and turbulence equations and 1×10^{-6} for energy and radiation equations. Heat fluxes and temperatures on all solid surfaces were recorded for analysis and discussion purposes.

3. Results and Discussion

3.1. Temperature Contours

Figure 4 shows the cavity temperature evolution during a day of July. As expected, the temperature inside the cavity increases until the solar midday due to the incoming solar radiation. After midday, the cavity temperature decreases both due to lower solar radiation and the heat absorbed by the VB louvers and convected to the water stream circulating through it.

Obtained average surface and cavity temperatures for the studied DSF-VB thermal collector system were in all cases lower than the values reported for DSF with mechanical air ventilation operating under similar climatic conditions [6,8,16]. These lower surface and cavity temperatures have a direct impact on the overall heat transfer toward the building, reducing the convective and radiative fluxes due to the reduction of the temperature gradient.

3.2. Heat Flux and Temperature Monitors

For each studied case, the total incident radiation (direct + diffuse + ground reflected) on the facade surface, the total (convection + radiation) heat rejected through the exterior glazing and the total (convection + radiation) heat entering the building was recorded for an average day of each month. The average surface temperatures of the VB louvers and both interior and exterior glazing, and the water outlet temperature were also recorded for each simulation run. Figures 5 and 6 show an example of the recorded heat fluxes and temperatures for south-facing DSF-VB during an average January day.

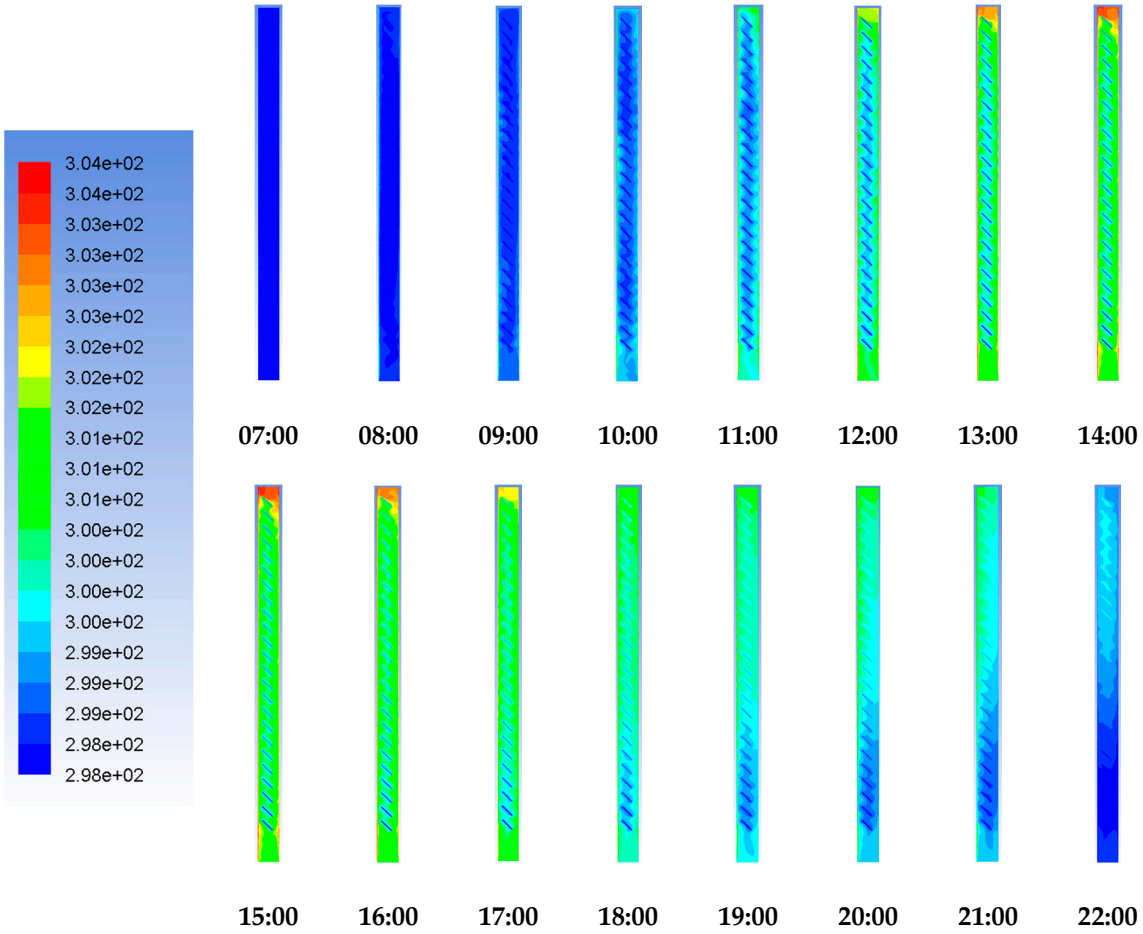

Figure 4. DSF cavity temperature evolution for an average July day for a south-facing DSF-Venetian blinds (VB) located in Barcelona (temperature scale in K).

As can be observed in Figure 5, the heat flux entering the building starts at sunrise and shows a max peak past the solar midday, when the cavity temperature is maximum. The heat rejected through the exterior glazing shows an initial value of about 235 W/m^2 at the start of the simulation (7:00 h) due to the temperature difference between the facade (initialized at 22 °C) and the outside air (around 8 °C).

Temperature evolution profiles shown in Figure 6 indicate that the interior glazing reaches a higher temperature than the exterior glazing. Although the exterior glazing gets all the incident radiation, it is a low-absorptivity/high-emissivity glass, leading to lower average temperatures. The interior glazing, on the other hand, is a low-emissivity glass that accumulates most of the heat it absorbs, hence the temperature increase.

Temperatures registered for both interior and exterior glazed surfaces for the DSF-VB thermal collector were found to be lower than those reported for a DSF or a DSF-VB under similar radiation conditions [22,35]. Water and VB louvers temperature increase during the day, due to the heat absorbed from the cavity. This behavior is reverted quickly after sunset, with no incident radiation (see Figure 4).

Figures 7 and 8 show an example of the recorded heat fluxes and temperatures for east/west-facing DSF-VB during an average April day. In general, the observed behavior is similar to that described for the south-facing facade but with a shorter exposition to solar radiation.

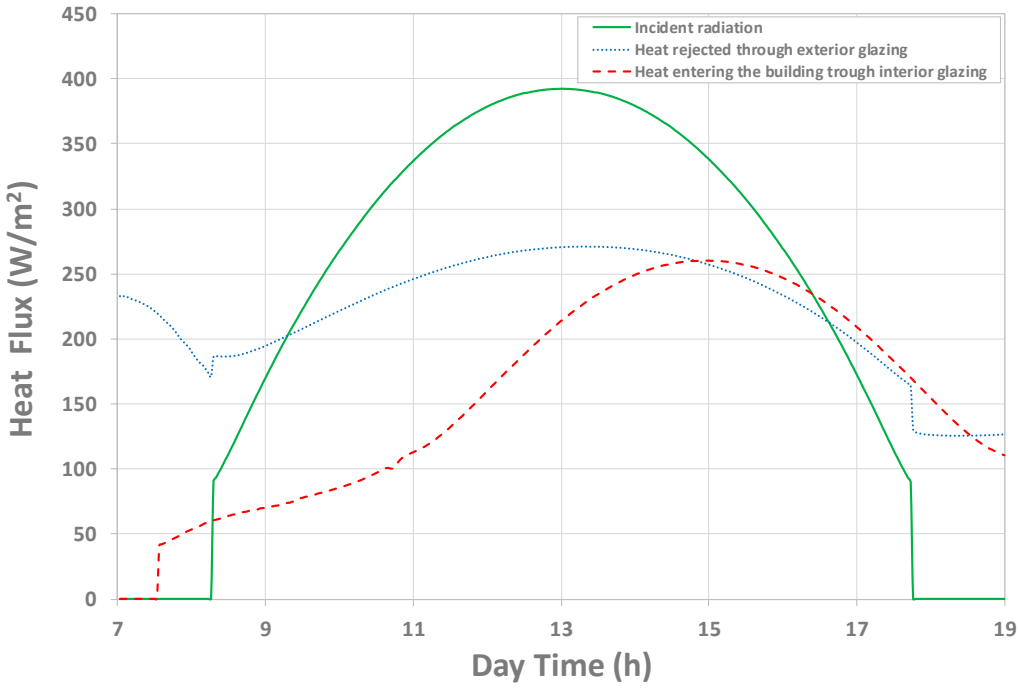

Figure 5. Heat fluxes recorded for a south-facing Double skin facade-Venetian blind (DSF-VB) located in Barcelona on an average January day.

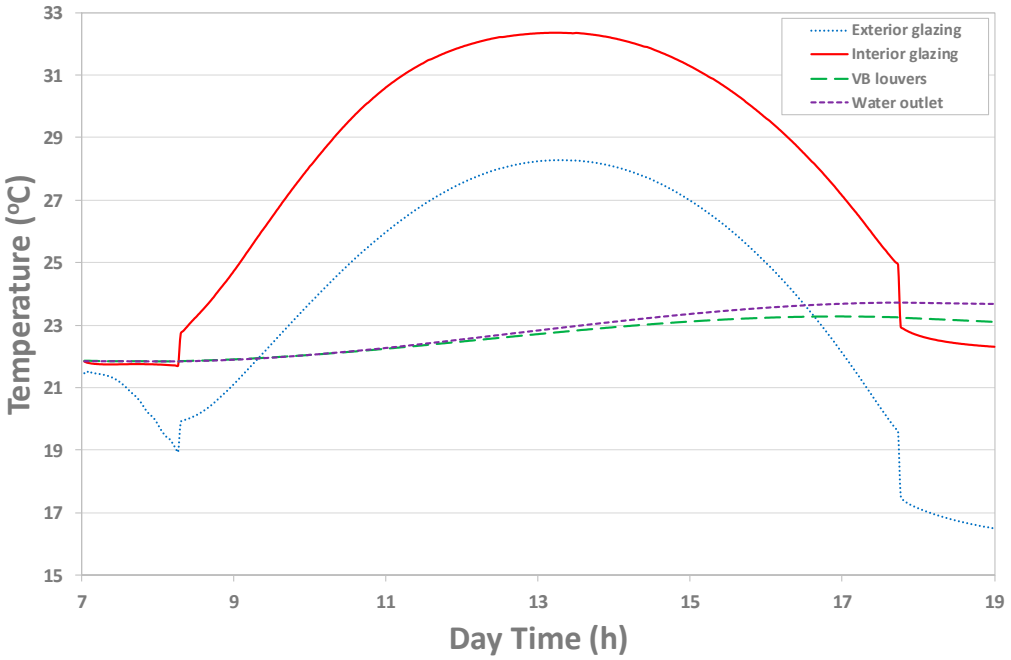

Figure 6. Temperatures recorded for a south-facing DSF-VB located in Barcelona on an average January day.

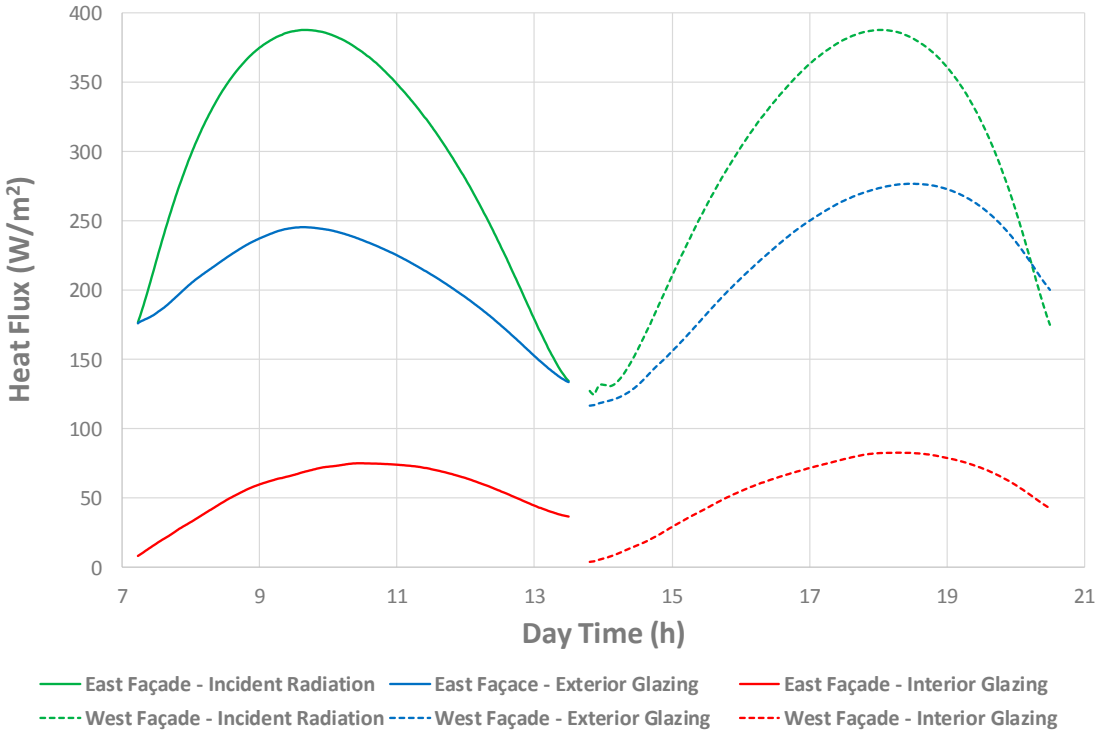

Figure 7. Heat fluxes recorded for east/west-facing DSF-VB located in Barcelona on an average April day.

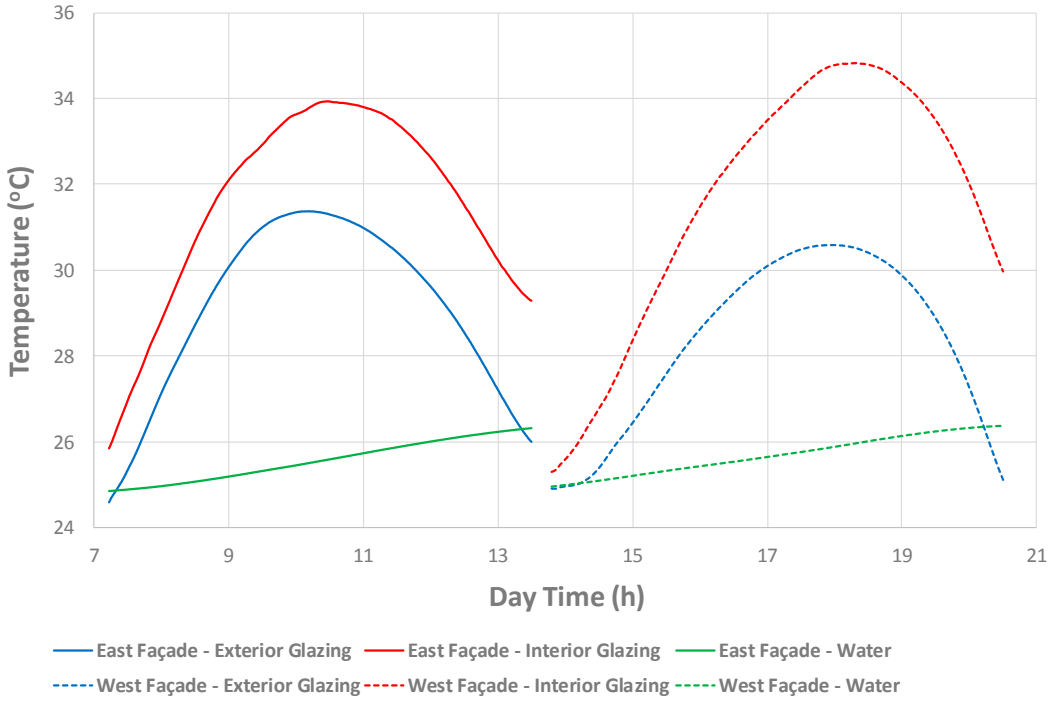

Figure 8. Temperatures recorded for east/west-facing DSF-VB located in Barcelona on an average April day.

3.3. Assessment of the Thermal Performance of the DSF-VB Thermal Collector

The purpose of the DSF-VB thermal collector is (as described in Section 2.1) to store the solar radiation absorbed by the VB louvers on a water stream circulating through the hollow slats, reducing the building solar heat gain and converting de facto the VB into a heat exchanger. In order to evaluate the performance of the VB thermal collector, two sets of simulations were run for each studied facade

(South, East, and West) with and without water circulation through the VB louvers. Heat fluxes vs day time were recorded at the exterior and interior glazing surfaces for all cases. For the DSF-VB Thermal Collector case, the heat flux through water inlet and outlet was also recorded. All heat fluxes recorded were integrated and area-weighted averaged to compute the incident radiation, the solar heat gains through the interior face of the inner glazing, and the heat recovered on the water stream.

Figures 9–11 show the evolution of the solar heat gains and the heat recovery for a year-round operation for the studied east, south and westbound facades respectively. It can be seen that using a VB type of structure to circulate water, effectively converting a DSF in a thermal collector, reduces the solar heat gains of the building.

For the eastbound (Figure 9) and westbound (Figure 11) facades, the evolution of solar heat gains and heat recovery is similar, with larger gains and recoveries from May to September, coinciding with the higher incident radiation and external temperatures experienced during the extended summer period. For the studied cases, a DSF-VB thermal collector improves the performance of a DSF-VB on east- and west-oriented facades, reducing solar heat gains by 28 to 40% when comparing the performance of a DSF-VB with and without water circulation.

For the southbound facade (Figure 10), it can be observed that both heat gains and heat recoveries are larger than those obtained for the east- and westbound facades, due to its larger exposition to solar radiation. For this facade, the reduction in solar heat gains range from 44 to 54% when comparing the performance of a DSF-VB with and without water circulation.

Table 5 shows the total values obtained for a yearlong operation of a DSF-VB thermal collector for the studied east, south and westbound facades. A thermal collector system improves the DSF-VB thermal performance by 11% (for east or west facades) to 23% (for the south facade). The west facade preforms slightly worse than the east facade due to a higher incident radiation and higher outside air temperatures registered in the afternoon when the west facade is exposed to direct solar radiation.

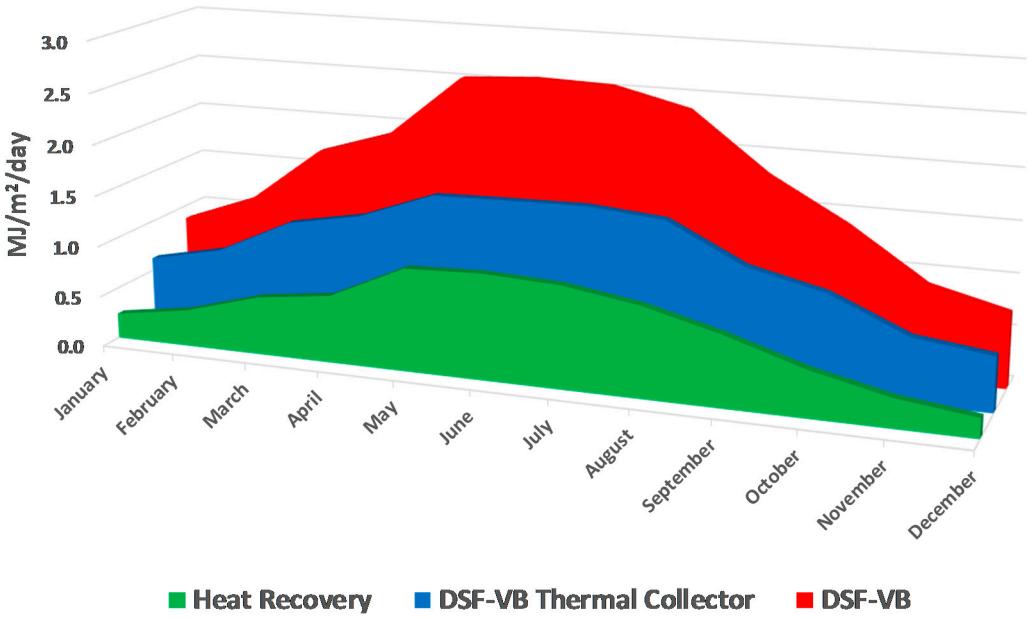

Figure 9. Year-round solar heat gains and heat recovery for an eastbound DSF-VB.

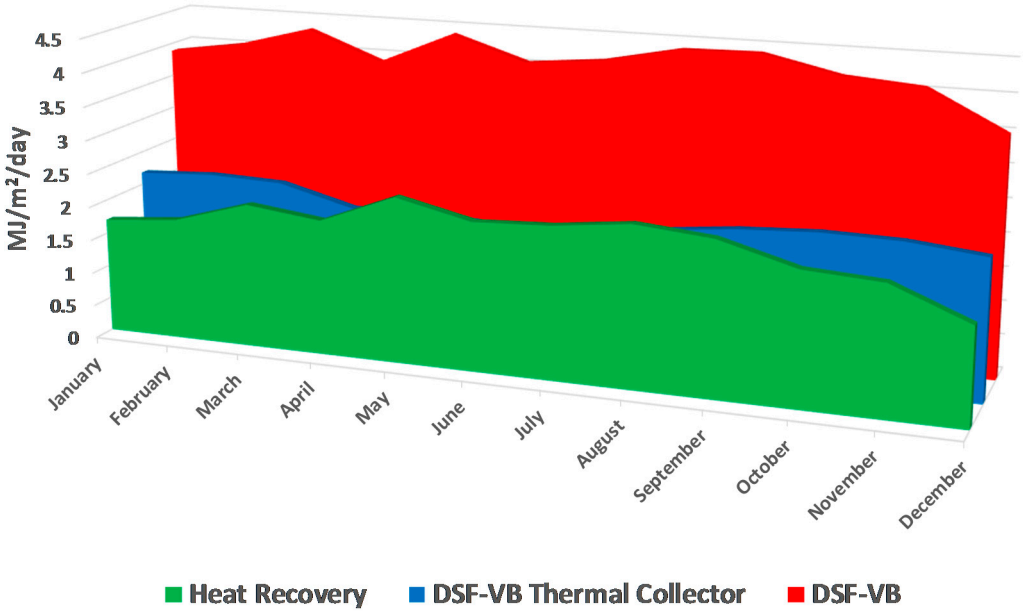

Figure 10. Year-round solar heat gains and heat recovery for a southbound DSF-VB.

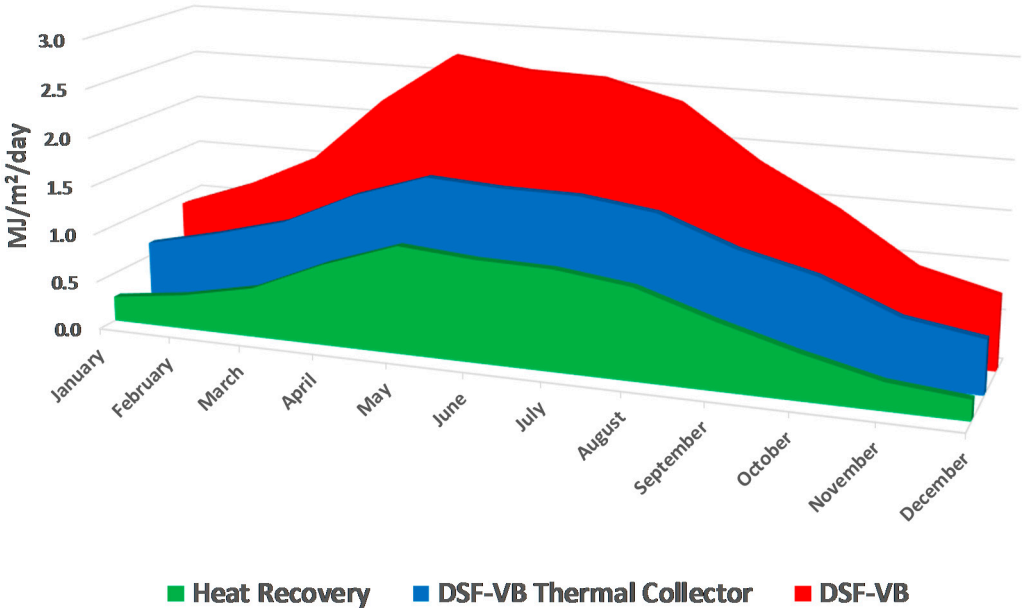

Figure 11. Year-round solar heat gains and heat recovery for a westbound DSF-VB.

Table 5. Recorded heat values for a yearlong operation.

MJ/m²/year	East	South	West
Incident Radiation	2057.59	3285.15	2120.27
Heat Gain DSF-VB	626.64	1506.44	645.70
Heat Gain DSF-VB Thermal Collector	402.16	759.44	410.65
Heat Recovery	224.48	747.00	235.05

4. Conclusions

CFD proves to be a useful tool when modeling conductive/convective/radiative heat transfer in DSF-VB modules. Numerical simulations were run for a yearlong operation of a DSF-VB module for an east-, west-, and south-oriented facade located in Barcelona, Spain.

For the studied cases, a VB-type of structure was included into a DSF module. This setup allows the facade to be used as a heat exchanger, where the absorbed radiation heat is convected into a water stream circulating inside the hollow aluminum slats that conform the VB.

Temperature fields together with heat fluxes through all surfaces were recorded for all studied cases. A previously validated modeling strategy [11] was used to obtain the presented results, consolidating the idea that CFD can offer tailored solutions for DSF-VB thermal collectors' performance assessment.

A parametric study was performed in order to evaluate the effect of certain parameters on the building solar heat gains. Lower solar heat gains were obtained when a higher water flow rate circulates through the DSF-VB thermal collector. In addition, heat gains were reduced by increasing the reflectivity of the cavity interior walls and by increasing the cavity width.

Heat fluxes through the interior glazing of a DSF-VB module with and without heat recovery were recorded to evaluate its thermal performance. For a yearlong operation, a DSF-VB thermal collector can reduce the solar heat gains to 19% (for the east/west facade) or to 22% (for the south facade) of the total incident radiation.

Comparing month-to-month operation, a DSF-VB thermal collector improves the performance of a DSF-VB by reducing solar heat gains by 28% (during winter) to 40% (during summer) when comparing the performance of an east or west-oriented DSF-VB with and without water circulation. For the south-oriented facade these reductions in solar heat gains range between 44% (during winter) and 54% (during summer) when comparing a DSF with and without water circulation.

Heat recovery on the DSF-VB module range from 11% (for the east- and west-oriented facade) and 22% (for the south-oriented facade) of the total incident radiation for a yearlong operation. Heat recovery is larger during the summer period for all studied facades. The thermal energy harvested could be used to partially cover the domestic hot water or heating (during winter) necessities of the building, reducing its primary energy consumption, and improving the building's carbon footprint.

Acknowledgments: The authors want to acknowledge the economic support from JG Grupo de Ingenieros Consultores for the development of this study. Access to the supercomputers property of Centre de Serveis Universitaris de Catalunya (CSUC) is also appreciated.

Author Contributions: A.G. and A.F. conceived and designed the numerical experiments. A.V. and S.J.G. performed the numerical experiments. A.F. and M.E. analyzed and consolidated the data. A.G. and M.E. wrote the paper.

Conflicts of Interest: The authors declare no conflict of interest.

Nomenclature

c_p	Specific heat	$J \cdot kg^{-1} \cdot K^{-1}$
k	Thermal conductivity	$W \cdot m^{-1} \cdot K^{-1}$
r	Louvers distance to outer glass	m
Re	Reynolds number	
t	Time	s
T	Static temperature	K
w	Cavity depth	m
Greek Letters		
α	Absorptivity	
β	Louvers tilt angle	
γ	Interior glazing reflectivity	
δ	Louvers thickness	m

ε	Emissivity	
λ	Louvers height	m
μ	Dynamic viscosity	$kg \cdot m^{-1} \cdot s^{-1}$
ρ	Fluid density	$kg \cdot m^{-3}$
τ	Transmissivity	

Acronyms

ASF	Active solar facade(s)
ASTF	Active solar thermal facade(s)
CFD	Computational fluid dynamics
DSF	Double skin facade(s)
DST	Daylight savings time
VB	Venetian blind(s)

References

1. Frankfurt School. FS-UNEP Collaborating Centre for Climate and Sustainable Energy Finance. In *Global Trends in Renewable Energy Investments 2017*; Frankfurt School of Finance and Management gGmbH: Frankfurt, Germany, 2017; Available online: http://fs-unep-centre.org/sites/default/files/publications/globaltrendsinrenewableenergyinvestment2017.pdf (accessed on 8 November 2017).
2. Pinel, P.; Cruickshank, C.A.; Beausoleil-Morrison, I.; Willis, A. A review of available methods for seasonal storage of solar thermal energy in residential applications. *Sustain. Energy Rev.* **2011**, *15*, 3341–3359. [CrossRef]
3. Brandl, D.; Mach, T.; Grobbauer, M.; Hochenauer, C. Analysis of ventilation effects and thermal behavior of multifunctional facade elements with 3D CFD models. *Energy Build.* **2014**, *85*, 305–320. [CrossRef]
4. Zhang, X.; Shen, J.; Hong, Z.; Wang, L.; Yang, T.; Tang, L.; Wu, Y.; Shi, Y.; Xia, L.; Xu, P.; et al. Building Integrated Solar Thermal (BIST) Technologies and Their Applications: A Review of Structural Design and Architectural Integration. *J. Fundam. Renew. Energy Appl.* **2015**, *5*, 182. [CrossRef]
5. Probst, M.C.M. Architectural Integration and Design of Solar Thermal Systems. Ph.D. Thesis, École polytechnique Fédérale de Lausanne, Lausanne, Switzerland, 2008.
6. Poirazis, H. *Double Skin Façades for Office Buildings*; Report EBD-R-04/3; Lund Institute of Technology, Lund University: Lund, Sweden, 2004.
7. Gratia, E.; de Herde, A. Optimal operation of a south double-skin façade. *Energy Build.* **2004**, *36*, 41–60. [CrossRef]
8. Guardo, A.; Coussirat, M.; Egusquiza, E.; Alavedra, P.; Castilla, R. A CFD approach to evaluate the influence of construction and operation parameters on the performance of active transparent façades in Mediterranean climates. *Energy Build.* **2009**, *41*, 534–542. [CrossRef]
9. Park, K.E.; Kang, G.H.; Kim, H.I.; Yu, G.J.; Kim, J.T. Analysis of thermal and electrical performance of semi-transparent photovoltaic (PV) module. *Energy* **2010**, *35*, 2681–2687. [CrossRef]
10. Mercado, L.V.; Addonizio, M.L.; Noce, M.D.; Veneri, P.D.; Scognamiglio, A.; Privato, C. Thin film silicon photovoltaics: Architectural perspectives and technological issues. *Appl. Energy* **2009**, *86*, 1836–1844. [CrossRef]
11. Li, D.H.W.; Lam, T.N.T.; Chan, W.W.H.; Mak, A.H.L. Energy and cost analysis of semi-transparent photovoltaic on office buildings. *Appl. Energy* **2009**, *86*, 722–729. [CrossRef]
12. Quesada, G.; Rousse, D.; Dutil, Y.; Badache, M.; Hallé, S. A comprehensive review of solar facades. Transparent and translucent solar facades. *Renew. Sust. Energy Rev.* **2010**, *16*, 2643–2651. [CrossRef]
13. Zhang, X.; Shen, J.; Lu, Y.; Xu, P.; Zhao, X.; Qiu, Z.; Zhu, Z.; Zhou, J.; Dong, X. Active solar thermal façades (ASTFs): From concept, application to research questions. *Renew. Sustain. Energy Rev.* **2015**, *50*, 32–63. [CrossRef]
14. Collins, M.R.; Harrison, S.J. Calorimetric analysis of the solar and thermal performance of windows with interior louvered blinds. *Trans. Am. Soc. Heat. Refrig. Air Cond. Eng.* **2004**, *110*, 474–485.

15. Guardo, A.; Egusquiza, M.; Egusquiza, E.; Alavedra, P. Preliminary results on the assessment of using Venetian blinds as a solar thermal collector in double skin facades in Mediterranean climates. In Proceedings of the 10th Conference on Advance Building Skins, Bern, Switzerland, 3–4 November 2015; EF Economic Forum: Munich, Germany, 2015; pp. 227–231.
16. Pasut, W.; de Carli, M. Evaluation of various CFD modelling strategies in predicting airflow and temperature in a naturally ventilated double skin façade. *Appl. Therm. Eng.* **2012**, *37*, 267–274. [CrossRef]
17. Manz, H. Total solar energy transmittance of glass double façades with free convection. *Energy Build.* **2004**, *36*, 127–136. [CrossRef]
18. Manz, H.; Schaelin, A.; Simmler, H. Airflow patterns and thermal behavior of mechanically ventilated glass double façades. *Build. Environ.* **2004**, *39*, 1023–1033. [CrossRef]
19. Safer, N.; Woloszyn, M.; Roux, J.J. Three-dimensinal simulation with a CFD tool of the airflow phenomena in a single floor double-skin façade equipped with a Venetian blind. *Sol. Energy* **2005**, *79*, 193–203. [CrossRef]
20. Ye, P.; Harrison, S.J.; Oosthuizen, P.H. convective heat transfer from a window with a Venetian blind: Detailed modelling. *Iashrae Trans.* **1999**, *105*, 1031.
21. Coussirat, M.; Guardo, A.; Jou, E.; Egusquiza, E.; Cuerva, E.; Alavedra, P. Performance and influence of numerical sub-models on the CFD simulation of free and forced convection in double-glazed ventilated façades. *Energy Build.* **2008**, *40*, 1781–1789. [CrossRef]
22. Parra, J.; Guardo, A.; Egusquiza, E.; Alavedra, P. Thermal performance of ventilated doublé skin façades with venetian blinds. *Energies* **2015**, *8*, 4882–4898. [CrossRef]
23. Selmi, M.; Al-Khawaja, M.J.; Marafia, A. Validation of CFD simulation for flat plate solar energy collector. *Renew. Energy* **2008**, *33*, 383–387. [CrossRef]
24. Villar Molero, N.; Cejudo López, J.M.; Domínguez Muñoz, F.; Rodríguez García, E.; Carrillo Andrés, A. Numerical 3-D heat flux simulations on flat plate solar collectors. *Sol. Energy* **2009**, *83*, 1086–1092. [CrossRef]
25. Martinopoulos, G.; Missirlis, D.; Tsilingiridis, G.; Yakinthos, K.; Kyriakis, N. CFD modelling of a polymer solar collector. *Renew. Energy* **2010**, *35*, 1499–1508. [CrossRef]
26. Missirlis, D.; Martinopoulos, G.; Tsilingiridis, G.; Yakinthos, K.; Kyriakis, N. Investigation of the heat transfer behaviour of a polymer solar collector for different manifold configurations. *Renew. Energy* **2014**, *68*, 715–723. [CrossRef]
27. Fan, J.; Shah, L.J.; Furbo, S. Flow distribution in a solar collector panel with horizontally inclined absorber strips. *Sol. Energy* **2007**, *12*, 1501–1511. [CrossRef]
28. Varol, Y.; Oztop, H. Buoyancy induced heat transfer and fluid flow inside a tilted wavy solar collector. *Build. Environ.* **2007**, *42*, 2062–2071. [CrossRef]
29. Gertzos, K.P.; Caouris, Y.G. Experimental and computational study of the developed flow field in a flat plate integrated collector storage (ICS) solar device with recirculation. *Exp. Therm. Fluid. Sci.* **2007**, *31*, 1133–1145. [CrossRef]
30. Henderson, D.; Junaidi, H.; Muneer, T.; Grassie, T.; Currie, J. Experimental and CFD investigation of an ICSSWH at various inclinations. *Renew. Sustain. Energy Rev.* **2007**, *11*, 1087–1116. [CrossRef]
31. Gilmore, D.G.; Stuckey, W.K.; Fong, M. Thermal surface finishes. In *Spacecraft Thermal Control Handbook*, 2nd ed.; Gilmore, D.G., Ed.; The Aerospace Press: El Segundo, CA, USA, 2002; Volume 1, pp. 139–159, ISBN 1-884989-11-X.
32. Servei Meteorològic de Catalunya. Available online: www.meteo.cat (accessed on 19 July 2017).
33. Ravello, A. Uso De La Radiación Solar En DFA Para La Reducción De Cargas De Enfriamiento. Bachelor's Thesis, Universitat Politècnica de Catalunya, Barcelona, Spain, 2017.
34. Ministerio de Energía, Turismo y Agenda Digital; Gobierno de España. Reglamento de Instalaciones Térmicas En Los Edificios. 2013. Available online: http://www.minetad.gob.es/energia/desarrollo/EficienciaEnergetica/RITE/Paginas/InstalacionesTermicas.aspx (accessed on 8 November 2017).
35. Guardo, A.; Coussirat, M.; Valero, C.; Egusquiza, E.; Alavedra, P. CFD assessment of the performance of lateral ventilation in double glazed façades in Mediterranean climates. *Energy Build.* **2011**, *43*, 2539–2547. [CrossRef]